Int J Adv Manuf Technol (2015) 77:1229–1247
DOI 10.1007/s00170-014-6540-x

ORIGINAL ARTICLE

Modeling and analysis of crater formation during wire electrical discharge turning (WEDT) process

Abimannan Giridharan · G. L. Samuel

Received: 4 July 2014 / Accepted: 20 October 2014 / Published online: 6 November 2014

Abstract Wire electrical discharge turning (WEDT) process is one of the emerging non-traditional machining processes for manufacture of micro- and axi-symmetric components. In WEDT process, material is removed by successive sparks that form craters. The material removal by crater formation is associated with energy supplied in the gap referred as discharge energy. This energy must be controlled for effective machining. In this paper, a model is proposed for predicting the crater diameter based on anode erosion. Finite element method (FEM) is used to simulate the crater for different plasma flushing efficiency. Effect of discharge energy developed in the gap, physio-thermal properties of the material are considered for modeling. The erosion energy required to form a crater is also evaluated using anode erosion model. The proposed models are validated by conducting WEDT experiments on high-tensile steel [AISI 4340]. The crater morphology is investigated by using images obtained from scanning electron microscope (SEM) and energy-dispersive X-ray analysis. The crater diameter predicted by anode erosion and FEM models are compared with diameter obtained from SEM micrograph. The results obtained from the proposed models are well in agreement with the experimental results. The anode erosion model predicts the crater diameter and erosion energy with an average absolute error of 5.65 and 17.86 %, respectively. By estimating the energy required to erode a material and by setting appropriate process settings, the discharge energy can be effectively utilized for material removal.

Keywords Wire electrical discharge turning · Discharge energy · Anode erosion model · Plasma flushing efficiency · Crater diameter · Erosion energy

A. Giridharan · G. L. Samuel (✉)
Indian Institute of Technology Madras, Chennai, India
e-mail: samuelgl@iitm.ac.in

Nomenclature

c_p	Specific heat capacity (joule per kilogram per degree Celsius)
$q(r)$	Heat flux (watts per square meter)
D	Diameter of crater (meters)
r	Radius of crater (meters)
E	Discharge energy (joules)
R	Radius of spark (meters)
E_e	Erosion energy (joules)
t	Time (seconds)
F_c	Constant fraction of total power
t_e	Discharge time (microseconds)
h_c	Convective heat transfer co-efficient (watts per square meter per degree Celsius)
T_0	Initial/ambient temperature (degree Celsius)
H_v	Enthalpy of vaporization (joules per kilogram)
T_m	Temperature at melting condition (degrees Celsius)
$i(t)$	Discharge current (amperes)
T_b	Temperature at boiling condition (degrees Celsius)
k	Thermal conductivity (watts per meter per degree Celsius)
$u(t)$	Discharge voltage (volts)
L_m	Latent heat of melting (joules per kilogram)
V_c	Volume of crater (cubic meter)
L_v	Latent heat of vaporization (joules per kilogram)
ρ	Density of material (kilograms per cubic meter)

1 Introduction

Electrical discharge machining (EDM) is an electro-thermal non-traditional machining process with complex metal removal mechanism, through formation of plasma channel between the tool and work piece electrodes for electric flow, causing melting and evaporation of the work piece material.

Wire-electro discharge machining (Wire-EDM or WEDM) is one of the important non-traditional machining processes used for machining of difficult-to-machine materials and especially intricate profiles. Among the configurations of WEDM wire electrical discharge turning (WEDT) is an emerging area developed to generate cylindrical forms on hard and difficult-to-machine materials by adding a rotary axis.

The electrical discharges in the EDM process is highly complex and stochastic in nature, and involves a combination of several disciplines such as electric, magnetic, thermal, mechanic, dynamic, or hydraulic. Modeling of EDM process is quite difficult due to non-linear relationship between the input process parameters and output performance parameters [1, 2]. Several researchers have proposed theoretical model for predicting the crater dimension in EDM and WEDM process. Erden and Kaftanoglu [3] proposed a theoretical hypothesis to predict the behavior of materials for different energy functions and obtained an optimum energy function for achieving higher material removal rate. Wong et al. [4] attempted to measure power dissipated in the gap directly using micro-computer-based instrumentation and proposed a theoretical hypothesis for power during EDM process. Researchers proposed model based on plasma channel growth to predict crater diameter, thickness of thermally damaged layer and relative electrode wear with limited experimental results [5, 6]. Temperature-dependent material properties and a one-dimensional heat flow point heat source were employed to predict the crater diameter considering only the melting phenomena and compared with limited experimental results. However, the effect of vaporization is neglected [1, 7]. The shape of crater, Material Removal Rate (MRR), and roughness is predicted using the temperature developed on the workpiece, and observed erosion rate increases with increase in current density [8–10]. An experimental study states that the crater diameter, MRR, roughness, surface crack density, and recast layer thickness increases with increase in discharge energy [2, 11, 12]. Wang and Han [13] simulated the debris and bubble moment for consecutive pulse discharge in the machining gap and stated as the discharge current increases the bubbles moved to the outlet of the side gap decreases. Various thermal models proposed for predicting crater diameter in EDM have over-predicted the results compared with the experimental values due to simplifying assumptions like uniform distribution of heat flux, constant spark radius, neglecting the effect of vaporization, etc.

A simple computational model is developed to predict the failure of wire due to thermal load using input power, pulse on-time, wire velocity, and wire diameter [14]. Researchers proposed model to predict the temperature developed along the wire for varying cutting conditions, and stated maximum temperature is developed at the exit of the wire region [15, 16]. Spur and Schonbeck [17] developed a model to predict the crater depth and diameter using heat flux and stated the radius of crater and molten volume increases with increase in discharge time. Models based on process parameters were proposed for predicting crater dimension, and stated crater depth increases with increase in crater diameter [18, 19]. An attempt has been made to model the cutting speed, surface roughness and waviness using response surface methodology (RSM) and artificial neural network using WEDM input parameters like pulse on time, pulse off time, wire tension, and dielectric flushing pressure [20]. The influence of WEDM process parameters on specific discharge energy of different materials is studied and found that the discharge efficiency is higher for smaller discharge gap [21].

Researchers have contributed to machining of cylindrical components using WEDT process. Turning of small pins of 5 μm diameter and micro-spindles using WEDM can be used for miniature products with roughness and dimensional accuracy of the order of 10 nm [22]. An attempt has been made to study the feasibility of cylindrical wire EDM process for high material removal and assessed the possible surface finish and roundness in producing free-form geometries using WEDM process [23, 24]. Authors have studied the effects of power, pulse off time, voltage, and spindle rotational speed on MRR, roughness, and roundness of the machined parts using RSM in cylindrical WEDT process [25, 26]. A pulse discriminating algorithm has been proposed for classifying open circuit, normal, arc, and short circuit pulses with a comparative study on the influence of process parameters on WEDM and WEDT processes [27]. Most of the work on crater formation or associated morphology is based on one-dimensional heat conduction equation validated with limited experimental data. Also, the effect of vaporization on crater formation is neglected. Not much work is carried out in modeling crater diameter in wire electrical discharge turning process.

In the present work, anode erosion model and finite element modeling (FEM) are developed to predict the crater diameter using physical and thermal properties of the work material. Using anode erosion model, the energy required to erode the material and form a crater is evaluated. The proposed models are verified by conducting WEDT experiments varying process parameters such as pulse off time, servo feed, and spindle rotation. The effect of discharge energy during WEDT process on crater morphology of the machined components is investigated. The crater morphology is analyzed by using images obtained from scanning electron microscope (SEM). The details of models, experiments carried out, and the results obtained are presented in this paper.

2 Theoretical model for predicting crater diameter and erosion energy

2.1 Anode erosion model

It is a known fact that each discharge removes a very small amount of material during WEDT process, and after a cumulative number of discharges, a desired amount of material is removed. The energy supplied in the inter-electrode gap during the discharge is transformed into heat energy. During the erosion process, the input parameter is discharge energy, and it is required to find a correlation between erosion at the electrodes and the energy inputs at the anode and cathode zones, with due consideration to the latent heats of change of state [28]. The following assumptions were made to develop a model for predicting crater diameter.

1. Each pulse results in formation of a crater.
2. All pulses are assumed to be normal erosion pulse, and the energy required to form a crater is same for all the pulses, i.e., the effect of inactive pulses such as short-circuit and open voltage are neglected.
3. The fraction of discharge energy going into work piece is assumed to be constant during the pulse.
4. The heat generated during discharge is transmitted into the work piece by conduction. The convective and radiation heat transfer coefficients are assumed to be negligible.
5. The average thermo-physical properties of the steel material are assumed to be constant in all three phase solid, liquid, and vapor [7]. The average thermo-physical properties are given in Table 1. The enthalpies of phase change are neglected [29]
6. The work piece material is homogeneous and isotropic [29]
7. In the present work, the boiling temperature of steel (2,886 ° C) and stainless steel (3,000 ° C) are close; the latent heat of vaporization of stainless steel is used [29]

At the interface separating the solid and the liquid phases, energy is liberated or adsorbed at a rate proportional to the volumetric rate of conversion of the material (dV_c/dt), and that energy must be balanced by the energy flow from the interface represented by the Eq. 1 [7].

$$F_c VI = \rho L_m \frac{dV_c}{dt} \tag{1}$$

Where F_c is the constant fraction of total power VI, ρ is density, and L_m is latent heat of melting.

In Eq. 1, only a fraction of discharge energy (18 %) is considered as effective energy utilized for removal of material, and the effects of vaporization is not considered. The debris and metallic particles expelled from the electrodes can be grouped under two categories. First, solid spheroids, resulting from the removal of molten metal, was followed by a coalescence phenomenon. Second, hollow spheroids or shells are believed to be expelled in the vapor phase, each forming a bubble in the cool dielectric and thus condensing rapidly enough to take on the geometry of the bubble [28].

The discharge energy delivered by each pulse is taken as the input parameter, and the effect of vaporization is also considered while predicting the crater diameter using physio-thermal property of the material. Hence, the equation proposed by Dibitonto et al. [7] is modified as Eq. 2 for predicting the volume of crater (V_c) as

$$V_c = \frac{0.18E}{\rho(L_m + L_v)} \tag{2}$$

Where V_c is volume of crater, E is discharge energy for single pulse, ρ is density of the material and L_m & L_v are latent heat of melting and vaporization.

In this wok the discharge energy is computed from voltage and current pulse trains acquired using digital storage oscilloscope. The discharge energy for single pulse is given by the Eq. (3) [2]

$$Energy(E) = \int_0^{t_e} u(t)i(t)dt \tag{3}$$

The crater is assumed to be of hemi-spherical shape, and the radius of crater is determined as

$$V_c = \frac{2}{3}\pi r^3 \tag{4}$$

Where r is the radius of crater. Combining Eqs. 2 and 4, we get

$$r = \left[\frac{0.086E}{\rho\,(L_m + L_v)}\right]^{\frac{1}{3}} \tag{5}$$

Table 1 Average thermo-physical property of steel material

Thermo-physical property	Values
Density (ρ)	7,545 kg/m^3
Specific heat capacity (C_p)	575 J/(kg °C)
Melting temperature (T_m)	1,535 °C
Boiling temperature (T_b)	2,886 °C
Latent heat of melting (L_m)	247 kJ/kg
Latent heat of vaporization (L_v)	6,500 kJ/kg

The diameter of crater is predicted from the following cubic equation

$$D = 2 * \left[\frac{0.086E}{\rho(L_m + L_v)}\right]^{\frac{1}{3}} \quad (6)$$

The actual energy used to erode the material to form a crater by considering vaporization is given by Eq. 7, the product of volume of crater, density of material, and enthalpy of vaporization [29].

$$E_e = V_c \rho H_v \quad (7)$$

Where E_e is erosion energy required to form crater, and H_V is enthalpy of vaporization. From thermodynamics, the energy necessary to vaporize a given amount of metal is given by the following Eq. 8 [12]:

$$H_v = \int_{T_o}^{T_m} c_p\, dT + L_m + \int_{T_m}^{T_b} c_p\, dT + L_v \quad (8)$$

In this approach, the V_c and H_V in Eq. 7 is replaced by Eqs. 2 and 8, respectively. The equation for evaluating the erosion energy based on anode erosion model is given by

$$E_e = \left[\frac{0.18E}{(L_m + L_v)}\right]\left[\int_{T_o}^{T_m} c_p\, dT + L_m + \int_{T_m}^{T_b} c_p\, dT + L_v\right] \quad (9)$$

2.2 Thermal modeling with finite element method

In EDM, the tool and work piece are immersed in the dielectric liquid, separated by a small gap. Application of voltage pulses across the small gap gives rise to electrical breakdown of the dielectric. The breakdown arises from the acceleration towards the anode of both the electrons emitted from the cathode by applied electric field and the stray electrons present in the gap. These electrons collide with neutral atoms of the dielectric, thereby creating positive ions and further electrons, which in turn are accelerated towards the cathode and anode, respectively. When the electrons and positive ions reach the anode and cathode, they give up their kinetic energy in the form of heat [30, 31]. In WEDM and WEDT, the erosion mechanism is same as that of EDM; the only difference is in WEDM the continuously travelling wire electrode is used as the tool, and an additional rotary axis is given to the work piece in WEDT process. However, in WEDM, pulses are of short duration with a highly transient discharge current [17]. For thermal analysis of WEDT process, conduction is considered to be the mode of heat transfer. Apart from assumptions in section 2.1, the following are used to develop this model for predicting crater diameter during WEDT process.

1. The shape of the heat source is assumed to be Gaussian distribution. The incident of heat flux on the domain is assumed to be axisymmetric.
2. The boundaries far from the region of spark is assumed to be insulated boundary.
3. During discharge, the material in the super-heated region is removed completely, and only a fraction of molten material is removed at the end of discharge.

2.2.1 Governing equation

The three-dimensional transient heat conduction equations with no heat generation are taken for thermal analysis of WEDT process, which can be given as

$$\frac{1}{r}\frac{\partial}{\partial r}\left(kr\frac{\partial T}{\partial r}\right) + \frac{1}{r^2}\frac{\partial T}{\partial \varnothing}\left(k\frac{\partial T}{\partial \varnothing}\right) + \frac{\partial}{\partial z}\left(k\frac{\partial T}{\partial z}\right) = \rho c_p \frac{\partial T}{\partial t} \quad (10)$$

Where r, z, Ø are the co-ordinates of cylindrical work domain; T is the temperature; k is thermal conductivity; ρ is density; and c_p is specific heat capacity of work piece material. The domain considered for analysis is assumed to be of axisymmetric $\frac{\partial T}{\partial \varnothing} = 0$.

Therefore Eq. 10 becomes

$$\frac{1}{r}\frac{\partial}{\partial r}\left(kr\frac{\partial T}{\partial r}\right) + \frac{\partial}{\partial z}\left(k\frac{\partial T}{\partial z}\right) = \rho c_p \frac{\partial T}{\partial t} \quad (11)$$

2.2.2 Boundary and initial conditions

A small cylindrical portion of the work piece around the spark is selected as domain. Figure 1 shows the schematic representation of thermal model used for WEDT process comprises of four boundaries (B_1, B_2, B_3, and B4). Top surface B_1 of work piece is subjected to heat flux up to sparking radius 'R' using Gaussian distribution, and beyond 'R' surface, B1 is in contact with dielectric medium; heat loss is modeled by using convective heat transfer. Boundaries B_2 and B_3 are far away from the spark zone that there is no heat transfer across them. Boundary B_4 is the axis of symmetry, as there is no heat gain, or loss heat flux is assumed to be zero. Therefore, the boundary conditions arewhen $t>0$

$$K(\partial T/\partial z) = \begin{cases} h_c(T - T_o) & r > R \\ q(r) & r \le R \quad \text{on } B_1 \\ 0 & \text{for pulse off-time} \end{cases} \quad (12)$$

$$\text{and} (\partial T/\partial n) = 0 \; on \; B_2,\; B_3,\; B_4 \quad (13)$$

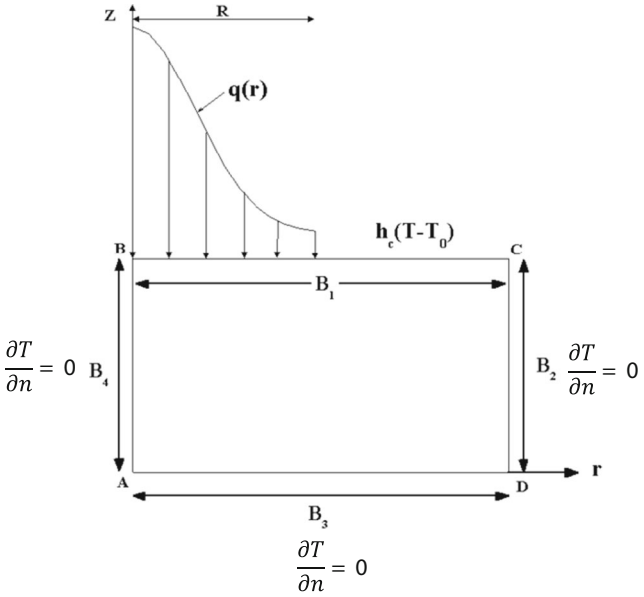

Fig. 1 Thermal model for WEDT process

Here, *q(r)* is the quantity of heat flux entering into the work piece, h_c is convective heat transfer co-efficient, T_o is the room temperature, and direction *n* is normal to boundary. The initial temperature T_a is taken as ambient temperature of the dielectric in which the domain is submerged. Therefore

$$T_a = T_o at\ t = 0 \tag{14}$$

2.2.3 Heat source

The important parameters which need to be considered for predicting the crater diameter are the fraction of heat input to the work piece, type of the heat source, and thermo-physical properties of the material. Researchers have attempted to predict the crater diameter assuming uniformly distributed heat source within a spark [5, 32] and point heat source [7]. Both these cases are simplistic as, in actual practice, neither a point heat source (like laser beam) nor any uniform (constant) application of heat on the work piece were there [1].

In the present work, Gaussian heat flux distribution is used to approximate the heat from plasma [33]. If the maximum heat flux q_0 at the axis of a spark and its radius *r* are known, then the heat flux $q(r)$ at radius *r* is given by

$$q(r) = q_0 \exp\left\{-4.5\left(\frac{r}{R}\right)^2\right\} \tag{15}$$

The maximum heat flux (q_0) can be calculated using the equation

$$q_0 = \frac{4.45 F_c V I}{\pi R^2} \tag{16}$$

where F_c is the fraction of energy transferred to work piece, *V* is discharge voltage, *I* is discharge current, and *R* is spark radius.

2.2.4 Energy distribution (F_c) factor

During EDM process, among the total energy dissipated in the gap, only a fraction of energy is been transferred/conducted through work piece; the remaining are lost to tool electrode and dielectric in the gap. From literature, different proposed values of energy distribution factor (F_c) are observed, ranging from 0.18–0.50 [5, 7, 34]. Spur and Schonbeck [17] approximated F_c to be 0.12. In this present work, the value of F_c is taken as 0.183, and its effect on crater diameter is analyzed [7].

2.2.5 Spark radius (R)

Spark radius is one of the important factors in thermal modeling of WEDT process. Experimentally, it is very difficult to measure the spark radius, since the arc plasma completes expanding within few microseconds after dielectric breakdown [35]. Various approaches have been proposed for finding the spark radius as a function of discharge duration. The plasma channel radius can be represented as product of constant defining the size of the plasma channel and discharge duration [10, 36] and also as a function of current rise time and thermo-physical properties of material [6, 17]. However, the spark radius is dependent on the discharge current and discharge duration. In this work, the spark radius is calculated by using the "equivalent heat input radius" [37],

$$R = 2040 I^{0.43} t_e^{0.44} \tag{17}$$

where *I* is discharge current and t_e is discharge time.

2.2.6 Metal removal efficiency and criterion for material removal

Metal removal efficiency or plasma flushing efficiency is total molten material removed from the molten pool at the end of pulse, while the remaining material resolidifies within the crater and its vicinity. Several authors carried out their modeling of EDM process considering the metal removal efficiency as 100 % [1, 33, 34]. In practice, it is not possible to achieve 100 % metal removal efficiency due to complexity and stochastic nature of EDM process. The metal removal efficiency of electrodes is varied between 2 and 96 % [7], 10–20 % [32], and 0.3–10 % [38–40] that resulted in over-prediction of metal removal compared with the experimental results. In this present work, the metal removal efficiency is taken as 3 %.

The criterion for metal removal (crater generation) is calculated based on the temperature distribution inside the work

piece on application of heat flux. In the present model, the melting temperature (T_m) of the work piece is taken as reference, and every element on the work piece that has reached the temperature higher than T_m will be removed.

2.2.7 Crater formation simulation steps

The simulation of crater formation is carried out by solving the governing Eq. 11 and employing boundary conditions in Eqs. 12 and 13 with Gaussian distributed heat flux as heat source for each spark of WEDT process. ANSYS™ 12.0 commercially available software for FEM analysis is used. A two-dimensional model of size 0.3×0.3 mm is developed for analysis. Four-noded, axisymmetric, thermal solid element (PLANE 55) was used [1]. Average physical and thermal properties of material thermal conductivity, specific heat capacity, and density of material were employed. ANSYS Parametric Design Language [41] was used to build the single spark WEDT model and repeated for different input process parameters. The following are the important steps adopted in determining the crater diameter

A model is created using PLANE 55 thermal solid element with fine mesh. Average physical and thermal properties of work material such as thermal conductivity, specific heat capacity, and density are applied. The initial and bulk temperatures are set as 298 K. Heat flux is applied at the region of spark. The temperature distribution is calculated for discharge duration. The elements and nodes above the melting temperature are identified and removed from mesh [1]. Figure 2 shows a typical temperature distribution, and Fig. 3 shows 2D axisymmetric expansion of a bowl-shaped crater geometry predicted by FEM model for AISI 4340 work material, discharge voltage 92 V, discharge current 2.5 A, and discharge duration 38 μs.

However, Fig. 3 represents the crater geometry predicted by FEM model with 100 % plasma flushing efficiency (ideal case). As stated earlier, in practice, only a fraction of molten material will be ejected from the melt pool. Therefore, only a fraction of total molten volume is used to predicting the final crater diameter. The following procedure is adopted to predict the actual crater diameter by taking into account the metal removal efficiency.

1. Using the above procedure, the ideal volume of crater for given process parameter is calculated using the radius and depth of crater.
2. Actual volume of crater is only a fraction of ideal volume of crater due to re-solidification of molten material. In this present work, the 1–4 % of metal removal efficiency is taken for consideration for finding the actual volume of crater.
3. Experimentally obtained crater on machined surface are measured at three different locations using SEM images.
4. The depth of crater is obtained from 3D topography of components machined under same process parameters conditions. Using this depth, the actual crater diameter is evaluated.

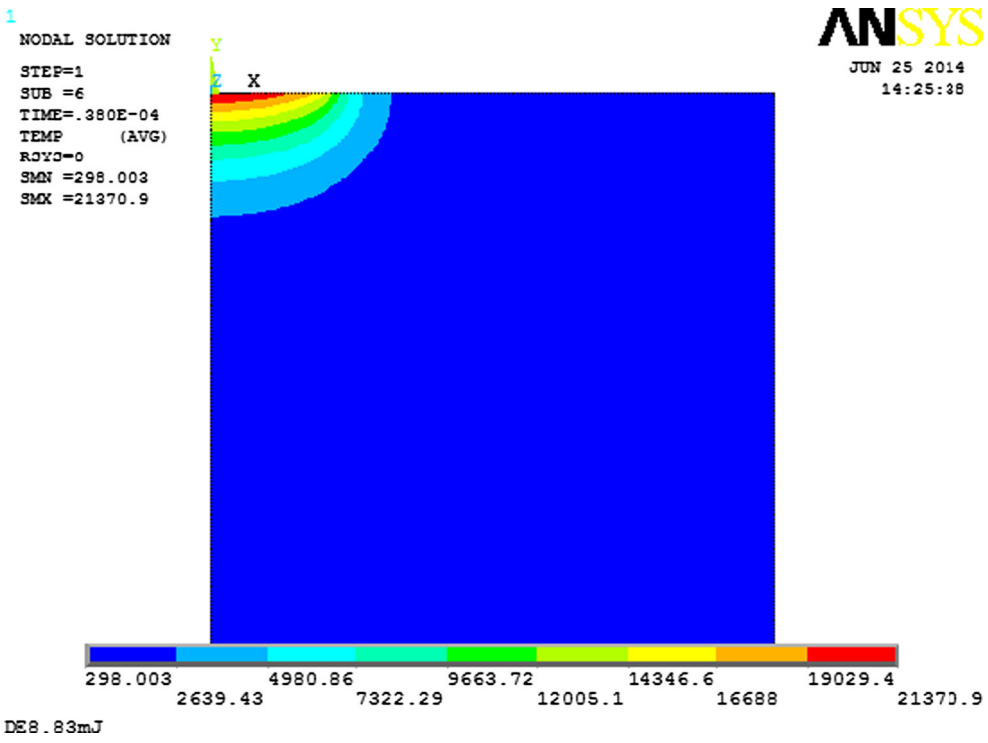

Fig. 2 Temperature distribution contour at the end of spark

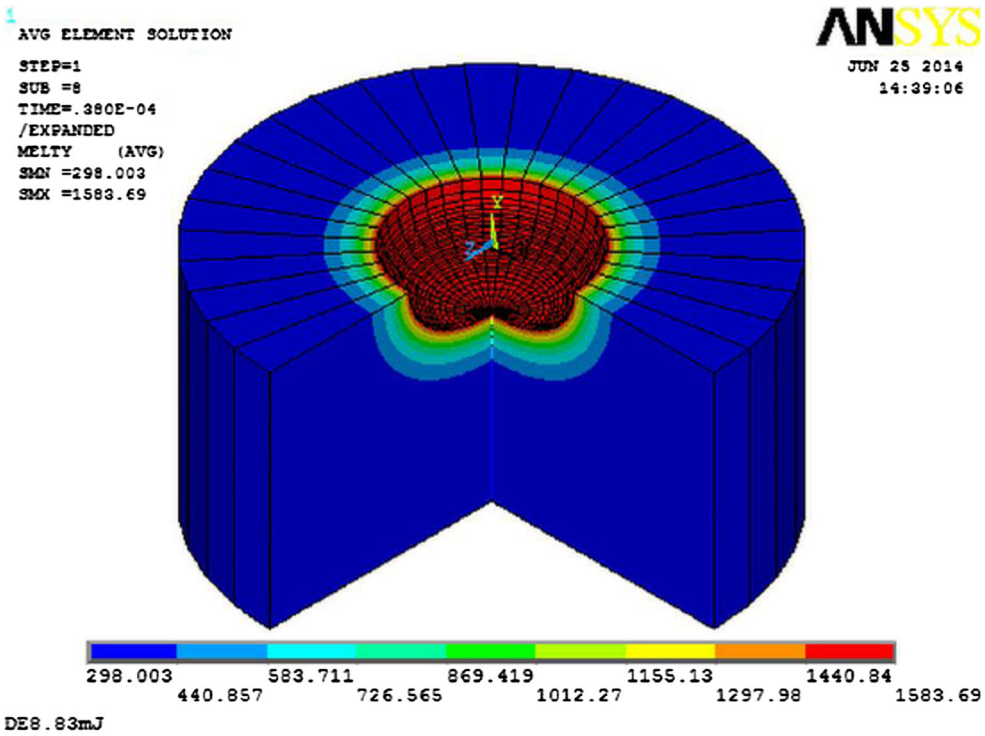

Fig. 3 Predicted shape of crater at end of spark using FEM analysis (radius, 60 μm; depth, 44 μm)

3 Experimental details

Experiments were conducted on Electronica ECOCUT machine with four controllable axes. Brass wire of diameter 0.25 mm was used as the electrode and deionized water as the dielectric medium. EN 24 [AISI 4340] high-tensile steel was used as the work piece material, considering its applications as heavy-duty axle shafts, pinions, torsion bars, etc. The chemical composition of the work piece is obtained using OES-ASTM E-415/99a test method, and their details are given in Table 2. An external rotary setup developed by Janardhan and Samuel [27] is used in the present work. The experimental setup is shown in Fig. 4. The parameters such as pulse off time can be varied from 9 to 42 μs, servo feed 0.5 to 11.5 mm/min, and spindle rotations from 3 to 98 rpm. These parameters were input parameters. The parameters were selected based on the preliminary experiments conducted in WEDM process. Above 8.2 mm/min of servo feed, the machining is inconsistent. Experiments were conducted by varying input parameters in five levels. Pulse off time of 9, 15, 28, 34, and 40 μs, servo feed of 0.5, 3.2, 5.0, 6.5, and 8.2 mm/min, and spindle rotation of 30, 45, 60, 75, and 90 rpm. Spark gap, wire feed, and depth of cut were maintained constant at 40 μm, 3 m/min, and 0.1 mm, respectively. In this work, the discharge energy is measured using Eq. 3.

Table 2 Chemical composition (wt%)

Steel	C	Mn	Si	S	P	Cr	Ni	Mo
EN 24	0.39	0.50	0.22	0.02	0.03	1.24	1.43	0.22

4 Results and discussion

4.1 Influence of process parameters on discharge energy

Discharge energy is calculated by Eq. 3, and influence of process parameters on discharge energy are given in Table 3.

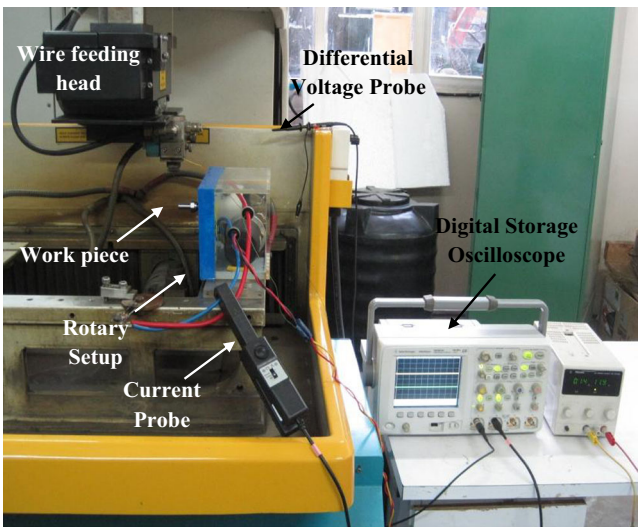

Fig. 4 Rotary setup and pulse train data acquisition system of WEDT process

Table 3 Experimental result on discharge energy

S. no.	Pulse off time (μs)	Servo feed (mm/min)	Spindle rotation (rpm)	Discharge energy (J)	No. of pulses per second	Discharge energy for single spark (mJ)
1	9	0.5	30	5.903	566	10.42
2			45	4.493	502	8.96
3			60	4.203	583	7.21
4			75	3.413	692	4.93
5			90	4.337	489	8.87
6		3.2	30	1.813	1,365	1.33
7			45	2.737	1,068	2.56
8			60	2.393	1,021	2.34
9			75	2.590	980	2.64
10			90	2.583	966	2.67
11		5.0	30	3.770	588	6.41
12			45	2.520	1,046	2.41
13			60	3.907	443	8.83
14			75	2.563	920	2.79
15			90	2.003	972	2.06
16		6.5	30	2.643	832	3.18
17			45	2.443	709	3.45
18			60	2.033	1,045	1.95
19			75	1.900	978	1.94
20			90	1.527	870	1.75
21		8.2	30	2.563	1,046	2.45
22			45	1.850	1,074	1.72
23			60	1.760	957	1.84
24			75	1.460	926	1.58
25			90	1.463	928	1.58
26	15	0.5	30	3.947	1,378	2.86
27			45	3.623	1,148	3.16
28			60	3.517	1,254	2.80
29			75	3.857	1,108	3.48
30			90	3.903	1,184	3.30
31		3.2	30	3.583	1,447	2.48
32			45	2.363	1,059	2.23
33			60	2.157	2,297	0.94
34			75	2.273	1,249	1.82
35			90	2.270	1,143	1.99
36		5.0	30	2.650	1,348	1.97
37			45	2.383	1,113	2.14
38			60	2.400	1,710	1.40
39			75	1.940	1,314	1.48
40			90	1.650	1,394	1.18
41		6.5	30	2.470	1,028	2.40
42			45	1.933	1,394	1.39
43			60	1.673	1,394	1.20
44			75	1.697	1,285	1.32
45			90	1.407	1,464	0.96
46		8.2	30	1.913	1,470	1.30
47			45	1.740	1,525	1.14
48			60	1.677	1,529	1.10

Table 3 (continued)

S. no.	Pulse off time (μs)	Servo feed (mm/min)	Spindle rotation (rpm)	Discharge energy (J)	No. of pulses per second	Discharge energy for single spark (mJ)
49			75	1.740	1,319	1.32
50			90	1.420	1,247	1.14
51	28	0.5	30	3.567	1,254	2.84
52			45	3.247	988	3.29
53			60	3.137	1,255	2.50
54			75	3.153	1,672	1.89
55			90	3.447	1,190	2.90
56		3.2	30	3.007	2,094	1.44
57			45	2.310	2,065	1.12
58			60	1.957	1,881	1.04
59			75	2.200	2,128	1.03
60			90	2.080	1,891	1.10
61		5.0	30	2.373	2,388	0.99
62			45	2.260	1,063	2.13
63			60	2.187	1,069	2.05
64			75	1.743	1,817	0.96
65			90	1.627	1,942	0.84
66		6.5	30	2.380	2,272	1.05
67			45	1.850	1,979	0.93
68			60	1.567	1,784	0.88
69			75	1.603	1,837	0.87
70			90	1.397	1,741	0.80
71		8.2	30	2.363	2,005	1.18
72			45	1.503	1,774	0.85
73			60	1.607	1,805	0.89
74			75	1.373	1,843	0.75
75			90	1.393	1,675	0.83
76	34	0.5	30	3.267	2,461	1.33
77			45	2.997	1,366	2.19
78			60	2.850	2,017	1.41
79			75	2.803	1,667	1.68
80			90	2.773	1,398	1.98
81		3.2	30	2.437	3,221	0.76
82			45	2.147	2,702	0.79
83			60	1.570	2,110	0.74
84			75	1.710	2,123	0.81
85			90	1.987	1,894	1.05
86		5.0	30	2.178	2,130	1.02
87			45	2.187	2,434	0.90
88			60	2.080	2,514	0.83
89			75	1.697	1,967	0.86
90			90	1.683	1,941	0.87
91		6.5	30	2.367	3,087	0.77
92			45	1.710	2,335	0.73
93			60	1.420	1,990	0.71
94			75	1.567	1,915	0.82
95			90	1.313	2,025	0.65
96		8.2	30	1.897	2,715	0.70

Table 3 (continued)

S. no.	Pulse off time (μs)	Servo feed (mm/min)	Spindle rotation (rpm)	Discharge energy (J)	No. of pulses per second	Discharge energy for single spark (mJ)
97			45	1.480	2,164	0.68
98			60	1.030	1,705	0.60
99			75	1.317	1,932	0.68
100			90	1.290	1,769	0.73
101	40	0.5	30	2.470	3,162	0.78
102			45	2.887	2,429	1.19
103			60	2.880	2,815	1.02
104			75	2.520	3,037	0.83
105			90	2.563	2,711	0.95
106		3.2	30	2.307	4,055	0.57
107			45	2.053	3,697	0.56
108			60	1.490	3,690	0.40
109			75	1.687	3,047	0.55
110			90	1.837	2,619	0.70
111		5.0	30	2.147	3,762	0.57
112			45	1.833	3,167	0.58
113			60	1.647	1,937	0.85
114			75	0.927	1,775	0.52
115			90	1.247	2,356	0.53
116		6.5	30	1.793	3,345	0.54
117			45	1.350	2,396	0.56
118			60	1.003	1,962	0.51
119			75	0.927	1,532	0.60
120			90	1.043	1,675	0.62
121		8.2	30	1.500	3,732	0.40
122			45	1.350	2,496	0.54
123			60	0.850	1,511	0.56
124			75	1.200	1,489	0.81
125			90	0.940	1,592	0.59

The energy level drops down with increase in pulse off duration. With increased pulse off duration—possibly formation of re-solidified/recast layer—the gap resistance can increase, resulting in gap energy drop. For all spindle rotation and pulse off duration, discharge energy is higher at 0.5 mm/min of servo feed and decreases at higher servo feed (5.0 and 8.2 mm/min). At lower servo feed of 0.5 mm/min, the average gap between the tool, and work piece is higher that leads to higher discharge energy in the gap as shown in Fig. 5. So, the discharge energy for individual pulse is higher at lower servo feed as given in Table 3. At higher servo feed (5.0 and 8.2 mm/min), the gap between the tool and work piece reduces, leading to arcing tendency. This results in reduction of discharge energy in the gap and individual pulse. For all servo feeds and pulse off time, with increasing spindle rotation, discharge energy decreases. As the spindle speed increases, a better flushing of the inter electrode gap occurs, maintaining a clean/clear dielectric environment. This results in reduced energy level as shown in Fig. 6. From Table 3, it is observed that, for a given pulse off time and spindle rotation, mostly increasing servo feed, the number of pulses acquired per second increases [27]. As the pulse off time increases, the capacitor discharges the more amount of charge stored in it, resulting in increased number of pulses. However, the magnitude of the individual power pulse reduces that resulted in reduced discharge energy in the gap as shown in Fig. 7. During machining, each spark results in formation of a crater both on wire (tool) and on the machined work piece. It is

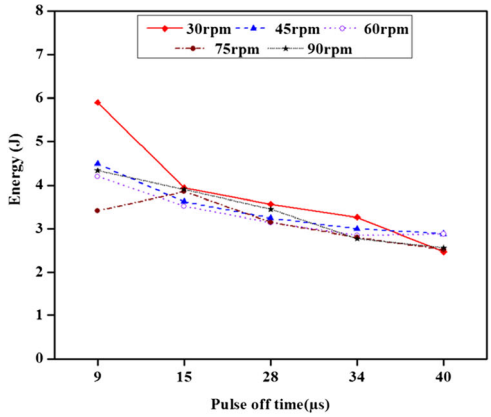

(a) 0.5 mm/min

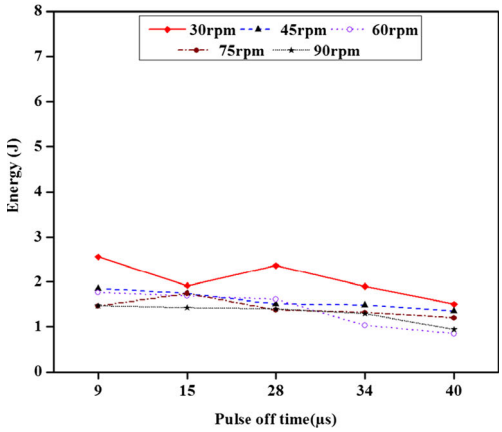

(b) 8.2 mm/min

Fig. 5 Effect of pulse off time on energy at different servo feed

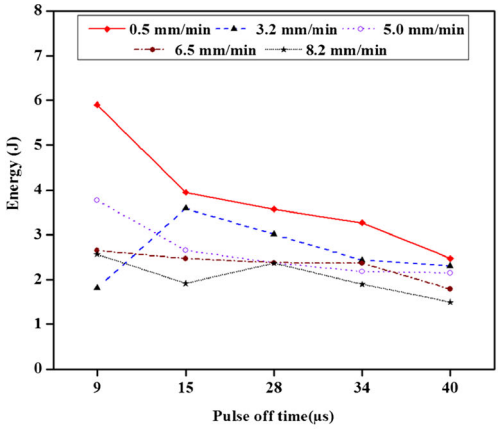

(a) 30 rpm

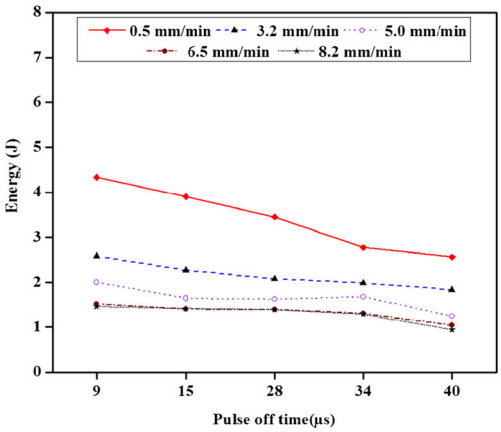

(b) 90 rpm

Fig. 6 Effect of pulse off time on energy at different spindle speeds

difficult to view increase in the number of pulses that results in formation of a crater on the machined work piece due to crater overlap [7, 20, 42]. The increase in the number of pulses can be seen on the spark-eroded wire electrode. For constant wire feed, increasing the servo feed from 0.5 to 8.2 mm/min, the increase in number of pulses can be seen from the SEM micrograph of the spark-eroded wire electrode. The micrograph of the spark eroded wire at a magnification of 500X is shown in Fig. 8. For a constant wire feed, the less number of sparks occurred at servo feed of 0.5 mm/min and more number of sparks occurred at 8.2 mm/min which resulted in crater overlap on the spark-eroded wire being viewed.

4.2 Influence of discharge energy on crater morphology

The morphology of crater formed during erosion as a function of discharge energy is studied using SEM. Each discharge results in the formation of a crater. The discharge energy supplied in the inter electrode gap is spent to heat, melt, and vaporize the electrode material. The SEM micrograph of the crater generated for different discharge energy is given in Fig. 9. Furthermore, it is observed that, the crater is shallow [11], and the diameter of crater (D) increases with increase in the discharge energy developed in the gap [19, 42, 43]. From the micrograph (Fig. 9), it is observed that the energy is effectively used in forming crater at low discharge energy compared with that of higher discharge energy. The diameter of crater is calculated from SEM micrograph [44] assuming the crater as the partially filled sphere. After the discharge ceases, the pressure, due to discharge over the molten metal, is removed, and pressurized gases expand and cause scattering of the molten metal away from the electrode surface. Scattered material droplets solidify in the cold dielectric liquid and form mostly global spheres. Spherical globules indicate the surface energy is minimum during solidification [45] as indicated in Fig. 9.

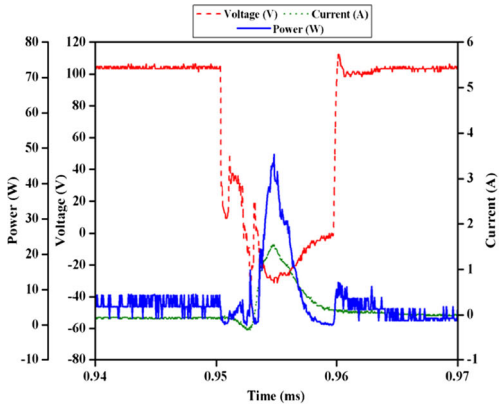

(a) At servo feed 0.5 mm/min

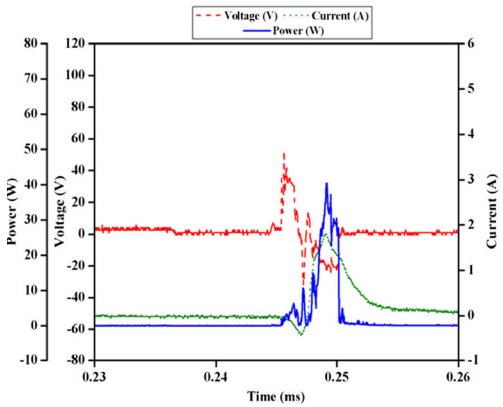

(b) At servo feed 8.2 mm/min

Fig. 7 Combined voltage, current, and power pulse train for normal pulse acquired at pulse off time 9 μs and spindle rotation 30 rpm

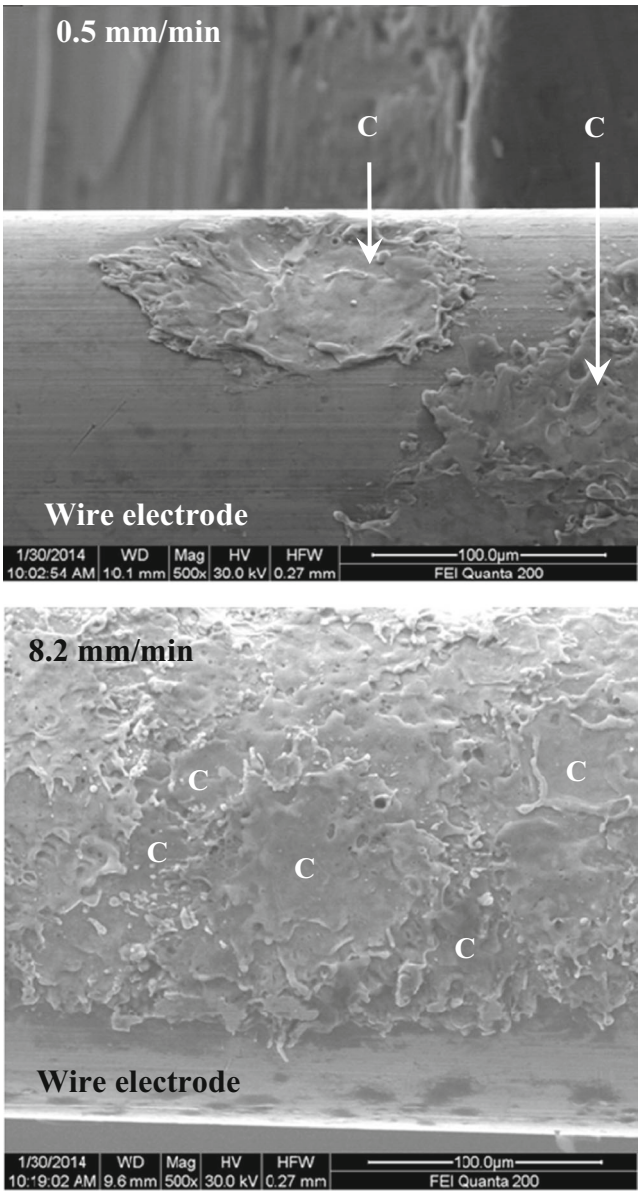

Fig. 8 SEM micrograph of spark-eroded wire electrode at different servo feed (*C* crater)

Apart from observation of crater morphology, possible chemical alterations/material responses to formation of crater are also assessed. Researchers have studied the possible chemical alterations on the machined surface using energy-dispersive X-ray (EDAX) and X-ray diffraction analysis during WEDM process [45–47]. In this wok, the chemical alteration undergone by a crater formed during WEDT process is studied through EDAX analysis. Typical EDAX profile of critical zone is illustrated in Fig. 10.

The area EDAX investigation is carried out on a localized crater. The energy dispersion profile (EDS) pertaining to region of observed crater is shown in Fig. 10 for component machined at pulse off duration of 9 μs, servo feed 5.0 mm/min, and spindle rotation 90 rpm. It is observed the presence of carbon or oxygen reduced amount of chromium that can be seen. This indicates possible depletion of chromium from material during crater formation. With 28 μs pulse off duration, tendency to arcing that leads to reduction in chromium (Cr, 0.70 wt%) or iron (Fe, 54.13 wt%). The amount of carbon (C, 8.41 wt%) and oxygen (O, 4.10 wt%) reduces. This may be attributed to possible depletion of Cr and dissociation of iron carbide (FeC). It is also observed that the percentage of oxygen is more at pulse off time 9 μs, servo feed 5.0 mm/min, and spindle rotation 90 rpm (8.37 wt%) compared with that of pulse off time 28 μs, servo feed 5.0 mm/min, and spindle rotation 90 rpm (4.10 wt%), and pulse off time 40 μs servo feed 5.0 mm/min, and spindle rotation 90 rpm (4.74 wt%). This can be attributed to the decomposition of water in the gap

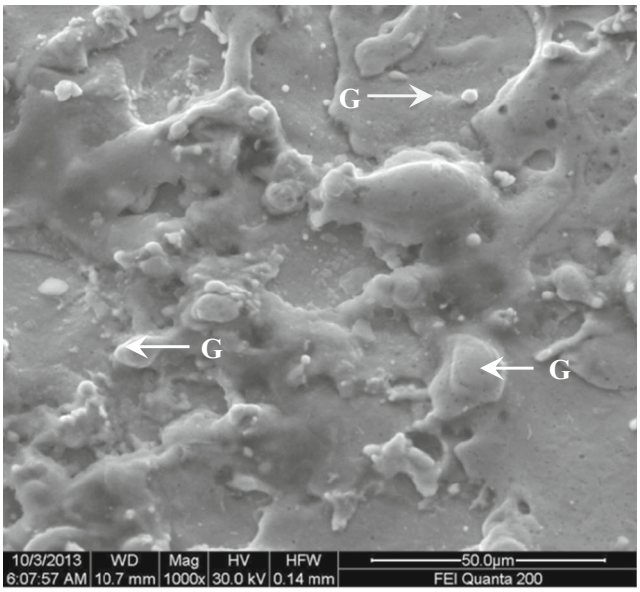

(a) Discharge energy 0.62 mJ (D =17µm)

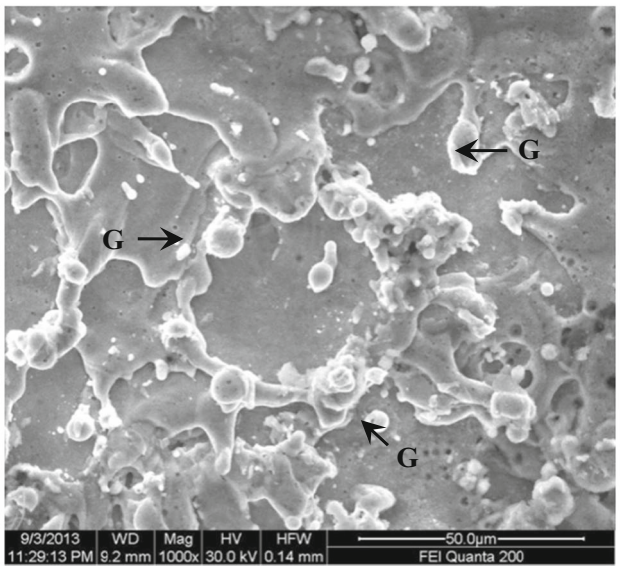

(b) Discharge energy 6.41 mJ (D =38µm)

Fig. 9 SEM micrograph of crater formed at different discharge energy for single pulse (*G*, globules)

at higher energy, resulting in increased percentage of oxygen [46]. With 40 µs pulse off duration, tendency of arcing, and vaporization of work piece material is splat-cooled (rapid cooling) and redeposit on the same crater which resulted in increased chromium (Cr, 1.07 wt%) and Iron (Fe 62.28 wt%). With increase in pulse off duration, a drop in discharge energy with a rise in number of pulses occurs. This results in increased arcing tendency. With increased arcing, the vaporized (eroded) material is splat-cooled (rapid cooling), and the presence of spherical globules supplements this.

4.3 Validation of proposed models

In order to validate the crater diameter predicted by anode erosion model and simulation results from FEM, five experimental data have been selected based on the discharge energy for single spark varying from high to low. Table 4 shows the details of machining parameters. The crater diameter is measured at three different locations, and their average value is given in Table 4.

In order to know the actual amount of metal removed for single spark during WEDT process, we have taken plasma flushing efficiency from 2 to 4 % for FEM model [40], and the results are compared with experimental data. The depth of crater is obtained by following the procedure given in section 2.2.7. Figure 11 shows the 3D surface topography and 2D cross-section of crater machined at 8.83 mJ of discharge energy. The 2D profile of one of the craters formed during machining is recorded and shown in Fig. 11b for determining the depth of the crater. The 3D surface topography and the 2D profile are captured using the BRUKER ContourGT machine. Figure 12 shows the comparison of crater diameter predicted by the proposed models (anode erosion model and FEM model) for different plasma flushing efficiency, with experimental results. It is observed that the results obtained from finite element modeling with 3 % plasma flushing efficiency matches well with the experimental results. From Fig. 12, it is also observed that the crater diameter predicted by the FEM model and anode erosion model are in good agreement. In next section, the anode erosion model is validated for predicting crater and erosion energy required to form that crater in detail.

4.3.1 Comparison of measured and predicted crater diameter

The crater diameter predicted by anode erosion model for different discharge energy varying from high to low using Eq. 6 is given in Table 5. Experimentally, the crater is measured at three different locations on machined component, and its average value is taken for comparison. For a given discharge energy, the predicted and measured diameter of crater for single pulse is given in Fig. 13. It is observed from Fig. 13 that anode erosion model clearly fits in with the measured/average crater size. From Table 5, it is observed that the anode erosion model predicts the diameter of crater with average absolute error of 5.65 %.

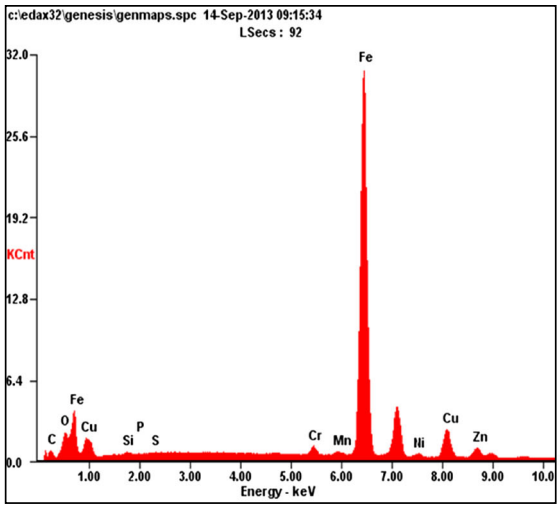

Fig. 10 EDS and SEM micrograph of component machined at pulse off time 9 μs, servo feed 5.0 mm/min, and spindle rotation 90 rpm (discharge energy, 2.003 J)

Element	*Wt%*	*At%*
CK	11.70	33.57
OK	08.37	18.03
SiK	00.44	00.53
PK	00.06	00.07
SK	00.15	00.16
CrK	00.85	00.56
MnK	00.48	00.30
FeK	64.07	39.52
NiK	00.71	00.42
CuK	08.68	04.71
ZnK	03.08	01.62
MoK	01.41	00.51
Matrix	Correction	ZAF

(a) EDAX properties of marked portion within crater

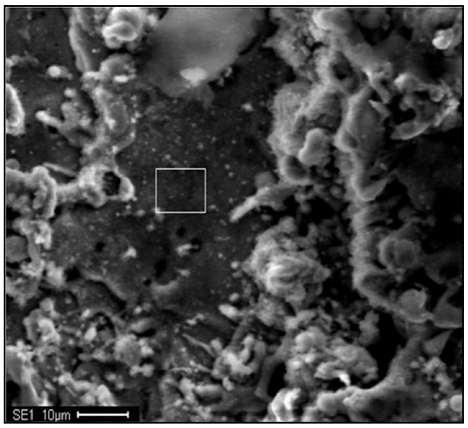

(b) SEM image of the machined component

4.4 Comparison of actual and evaluated erosion energy for single crater

The erosion energy required in forming a crater is calculated using Eq. 9, and the erosion energy required to form crater is given in Table 6.

The evaluated erosion energy and experimentally measured erosion energy to form crater is given in Fig. 14. It is observed at lower discharge energy for single pulse (less than 2.05 mJ) that the erosion energy for experimentally measured crater is higher than that of the evaluated erosion energy from the model. This is due to the

Table 4 Validation of anode erosion model and FEM model

Discharge energy (mJ)	Average voltage (V)	Average current (A)	Discharge duration (μs)	Measured average crater diameter (μm)	Height measured from 3D topography (μm)	Predicted crater diameter (μm)	
						Anode erosion model	FEM with [3 % PFE]
8.83	92	2.5	38	47	10	49.31	48.32
7.21	82	2	58	42	7	46.01	43.60
2.50	95	0.5	53	31	5	32.33	30.46
2.05	92	1	22	27	5	30.26	27.36
1.02	90	0.4	28	25	3	23.98	23.46

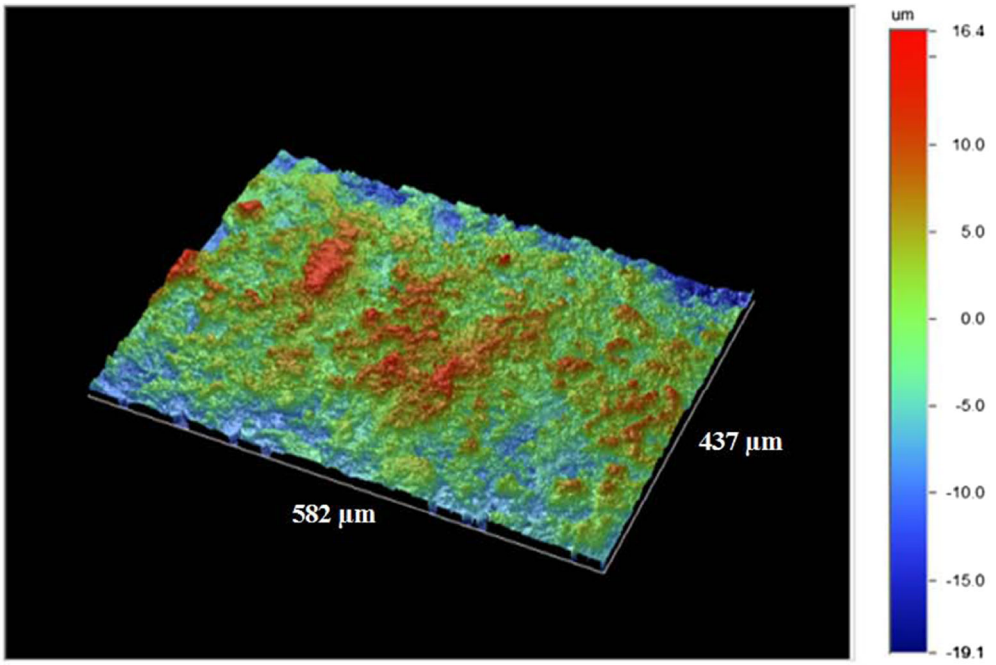

(a) 3D topography of machined surface

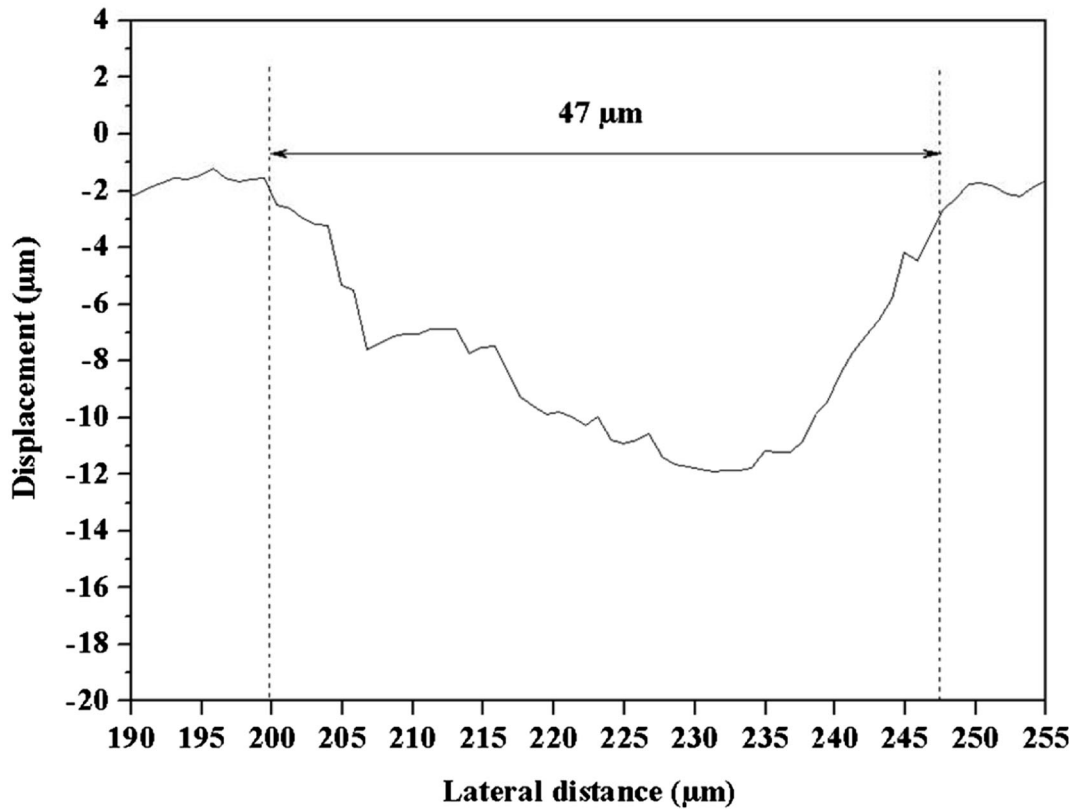

(b) 2D profile of a crater

Fig. 11 3D surface topography and 2D contour of a crater machined at 8.83 mJ of discharge energy

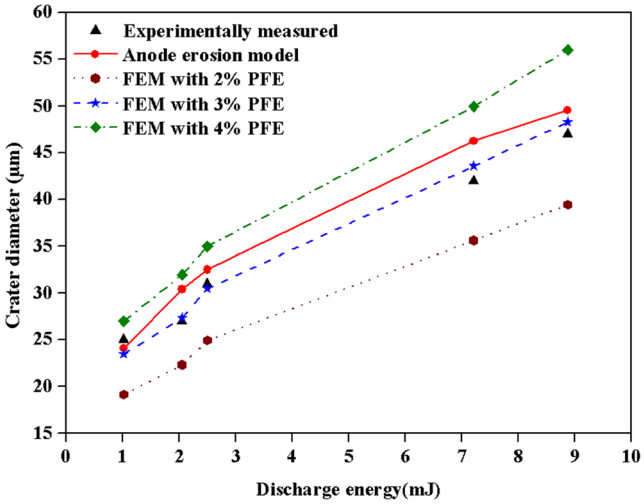

Fig. 12 Comparison of predicted crater diameter with experimental result

phenomenon of increase in number of pluses that resulted in crater overlap.

5 Conclusions

An energy-driven modeling to predict the diameter of crater and erosion energy required to form a crater using physio-thermal properties of the material is proposed. Also, the effect of input parameters such as pulse off time, servo feed, and spindle rotation on energy consumption is also assessed during wire electrical discharge turning process. The following are the important conclusions drawn from this work.

- An anode erosion model is developed to predict the crater diameter using discharge energy. Anode erosion model

Table 5 Comparison of measured and predicted crater diameter for given discharge energy

S. no.	Discharge energy for single pulse (mJ)	Measured crater diameter at different locations (μm)			Average crater diameter (μm)	Anode erosion model	
		Location 1	Location 2	Location 3		Crater diameter (μm)	Error (%)
1	8.87	43	49	49	47	49.31	−4.90
2	7.21	40	43	43	42	46.01	−9.56
3	6.41	38	45	51	45	44.25	0.94
4	3.48	34	37	40	37	36.09	2.45
5	3.29	32	32	34	33	35.43	−8.45
6	2.90	28	30	45	34	33.97	1.07
7	2.86	30	30	30	30	33.81	−12.70
8	2.84	30	34	34	33	33.73	−3.26
9	2.50	29	30	34	31	32.33	−4.28
10	2.45	28	33	37	33	32.11	1.70
11	2.19	32	30	30	31	30.93	−0.86
12	2.05	27	27	28	27	30.26	−10.70
13	1.48	24	32	39	32	27.14	14.28
14	1.41	29	34	29	31	26.71	12.91
15	1.33	23	24	34	27	26.19	2.99
16	1.30	21	28	27	25	26.00	−2.61
17	1.18	21	24	24	23	25.17	−9.43
18	1.14	23	24	29	25	24.88	1.78
19	1.02	24	24	27	25	23.98	4.09
20	0.95	17	17	31	22	23.41	−8.07
21	0.89	21	24	24	23	22.91	0.39
22	0.83	22	22	23	22	22.38	−0.23
23	0.78	15	21	23	20	21.93	−11.49
24	0.62	17	17	27	20	20.31	0.11
25	0.40	15	21	23	20	17.55	10.76
Average absolute error (%)							5.65

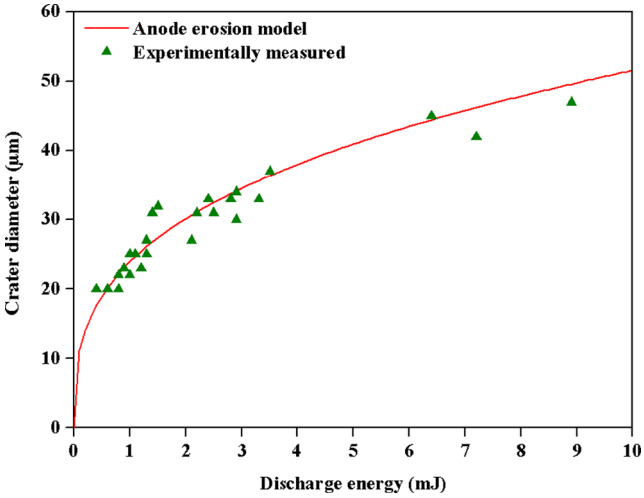

Fig. 13 Comparison of average measured and predicted diameter of crater

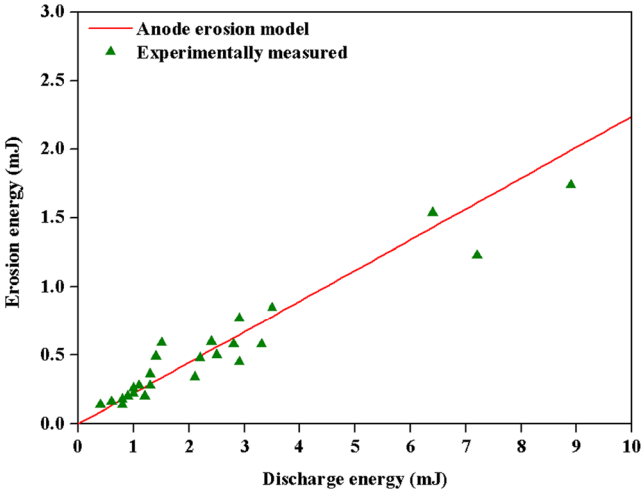

Fig. 14 Comparison of average measured and evaluated erosion energy to form crater

Table 6 Comparison of actual and evaluated erosion energy for a given crater

S. no.	Discharge energy for single pulse (mJ)	Erosion energy for craters measured on machined component at three different locations (mJ)			Average erosion energy for measured crater (mJ)	Anode erosion model	
		Location 1	Location 2	Location 3		Erosion energy (mJ)	Error (%)
1	8.87	1.32	1.95	1.95	1.74	1.99	−14.22
2	7.21	1.06	1.32	1.32	1.23	1.61	−31.06
3	6.41	0.91	1.51	2.20	1.54	1.44	6.74
4	3.48	0.65	0.84	1.06	0.85	0.78	8.37
5	3.29	0.54	0.54	0.65	0.58	0.74	−27.22
6	2.90	0.36	0.45	1.51	0.77	0.65	16.07
7	2.86	0.45	0.45	0.45	0.45	0.64	−43.14
8	2.84	0.45	0.65	0.65	0.58	0.64	−9.02
9	2.50	0.40	0.45	0.65	0.50	0.56	−11.75
10	2.45	0.36	0.60	0.84	0.60	0.55	8.50
11	2.19	0.54	0.45	0.45	0.48	0.49	−2.32
12	2.05	0.33	0.33	0.36	0.34	0.46	−35.53
13	1.48	0.23	0.54	0.98	0.59	0.33	43.35
14	1.41	0.40	0.65	0.40	0.49	0.32	35.11
15	1.33	0.20	0.23	0.65	0.36	0.30	17.43
16	1.30	0.15	0.36	0.33	0.28	0.29	−3.55
17	1.18	0.15	0.23	0.23	0.20	0.26	−29.61
18	1.14	0.20	0.23	0.40	0.28	0.26	8.27
19	1.02	0.23	0.23	0.33	0.26	0.23	12.64
20	0.95	0.08	0.08	0.49	0.22	0.21	2.79
21	0.89	0.15	0.23	0.23	0.20	0.20	2.25
22	0.83	0.18	0.18	0.20	0.18	0.19	−0.55
23	0.78	0.06	0.15	0.20	0.14	0.17	−27.49
24	0.62	0.08	0.08	0.33	0.16	0.14	14.82
25	0.40	0.06	0.15	0.20	0.14	0.09	34.62
Average absolute error (%)							17.86

predicts the crater diameter with an average absolute error of 5.65 % compared with experimental results.

- An attempt has been made to simulate the crater diameter using FEM for different plasma flushing efficiency. The influence of plasma flushing efficiency on crater diameter is analyzed, and it was observed that the crater diameter predicted by FEM closely matches with experimental results at 3 % of plasma flushing efficiency.
- In the present work, a new model is proposed for predicting erosion energy required to form the crater. The model predicts erosion energy to form a crater with an average absolute error of 17.86 %.
- A detailed analysis on the influence of discharge energy on crater morphology using SEM micrograph and EDAX analysis is carried out. The dimension of crater is measured using 3D topography of machined surface. The discharge energy produced in the gap to form a crater is effectively utilized at lower discharge energy than at higher discharge energy.
- The discharge energy decreases when increasing servo feed and spindle rotation for a fixed pulse off time. As the servo feed increased, more arcing occurs compared with sparking; this reduces energy. The increase in spindle rotation maintains a clear/clean dielectric environment which resulted in reduced discharge energy in the gap.

Using the model proposed in this work, it is possible to predict crater diameter before conducting the experiments. By selecting the suitable plasma flushing efficiency, closer prediction of crater diameter with experimental results can be achieved. By knowing the actual energy required to erode a given material, energy can be utilized effectively that leads to energy conservation during WEDT process. The proposed work can be applied for online monitoring of energy consumption and to achieve higher productivity (higher MRR with minimum energy consumption) while machining difficult-to-machine materials during WEDT process.

References

1. Joshi SN, Pande SS (2009) Development of an intelligent process model for EDM. Int J Adv Manuf Technol 45(3–4):300–317. doi:10.1007/s00170-009-1972-4
2. Gostimirovic M, Kovac P, Sekulic M, Skoric B (2012) Influence of discharge energy on machining characteristics in EDM. J Mech Sci Technol 26(1):173–179. doi:10.1007/s12206-011-0922-x
3. Erden A, Kaftanoglu B (1981) Thermo-mathematical modelling and optimization of energy pulse forms in electric discharge machining (EDM). Int J Mach Tools Des Res 21(1):11–22. doi:10.1016/0020-7357(81)90010-X
4. Wong YS, Edkins M, Noble CF (1987) An investigation of the power output and gap voltage during electrical discharge machining using microcomputer-based instrumentation. Int J Mach Tools Manuf 27(2):191–214. doi:10.1016/s0890-6955(87)80050-0
5. Jilani ST, Pandey PC (1983) An analysis of surface erosion in electrical discharge machining. J Wear 84(3):275–284. doi:10.1016/0043-1648(83)90269-7
6. Pandey PC, Jilani ST (1986) Plasma channel growth and the resolidified layer in EDM. Precis Eng 8(2):104–110. doi:10.1016/0141-6359(86)90093-0
7. Dibitonto DD, Eubank PT, Patel MR, Barrufet MA (1989) Theoretical models of the electrical discharge machining process. I. A simple cathode erosion model. J Appl Phys 66(9):4095–4103. doi:10.1063/1.343994
8. Singh A, Ghosh A (1999) A thermo-electric model of material removal during electric discharge machining. Int J Mach Tools Manuf 39(4):669–682. doi:10.1016/S0890-6955(98)00047-9
9. Salah NB, Ghanem F, Atig KB (2006) Numerical study of thermal aspects of electric discharge machining process. Int J Mach Tools Manuf 46(7–8):908–911. doi:10.1016/j.ijmachtools.2005.04.022
10. Izquierdo B, Sanchez JA, Plaza S, Pombo I, Ortega N (2009) A numerical model of the EDM process considering the effect of multiple discharges. Int J Mach Tools Manuf 49(3–4):220–229. doi:10.1016/j.ijmachtools.2008.11.003
11. Lee LC, Lim LC, Narayanan V, Venkatesh VC (1988) Quantification of surface damage of tool steels after EDM. Int J Mach Tools Manuf 28(4):359–372. doi:10.1016/0890-6955(88)90050-8
12. Wang BJ, Saka N, Rabinowicz E (1991) Static gap erosion of Ag-CdO electrodes. IEEE Transactions on Components, Hybrids, and Manufacturing Technology 14(2):374–385. doi; 10.1109/33.87318
13. Wang J, Han F (2014) Simulation model of debris and bubble movement in consecutive-pulse discharge of electrical discharge machining. Int J Mach Tools Manuf 77:56–65. doi:10.1016/j.ijmachtools.2013.10.007
14. Banerjee S, Prasad BVSS, Mishra PK (1993) A simple model to estimate the thermal loads on an EDM wire electrode. J Mater Process Technol 39(3–4):305–317. doi:10.1016/0924-0136(93)90165-3
15. Rajurkar KP, Wang WM (1993) Thermal modeling and on-line monitoring of wire-EDM. J Mater Process Technol 38(1–2):417–430. doi:10.1016/0924-0136(93)90214-Q
16. Hargrove SK, Ding D (2007) Determining cutting parameters in wire EDM based on workpiece surface temperature distribution. Int J Adv Manuf Technol 34(3–4):295–299. doi:10.1007/s00170-006-0609-0
17. Spur G, Schonbeck J (1993) Anode erosion in wire-EDM—a theoretical model. CIRP Ann 42(1):253–256. doi:10.1016/S0007-8506(07)62437-8
18. Tosun N, Cogun C, Pihtili H (2003) The effect of cutting parameters on wire crater sizes in wire EDM. Int J Adv Manuf Technol 21(10–11):857–865. doi:10.1007/s00170-002-1404-1
19. Han F, Jing J, Yu D (2007) Influence of discharge current on machined surfaces by thermo-analysis in finish cut of WEDM. Int J Mach Tools Manuf 47(7–8):1187–1196. doi:10.1016/j.ijmachtools.2006.08.024
20. Speeding TA, Wang ZQ (1997) Parametric optimization and surface characterization of wire electrical discharge machining process. Precis Eng 20(1):5–15. doi:10.1016/S0141-6359(97)00003-2
21. Liao YS, Yu YP (2004) Study of specific discharge energy in WEDM and its application. Int J Mach Tools Manuf 44(12–13):1373–1380. doi:10.1016/j.ijmachtools.2004.04.008
22. Masuzawa T, Tonshoff HK (1997) Three-dimensional micromachining by machine tools. CIRP Ann 46(2):621–628. doi:10.1016/S0007-8506(07)60882-8
23. Qu J, Shih AJ, Scattergood R (2002) Development of the cylindrical wire electrical discharge machining process, part 1: concept, design, and material removal rate. J Manuf Sci Eng 124(3):702–707. doi:10.1115/1.1475321
24. Qu J, Shih AJ, Scattergood R (2002) Development of the cylindrical wire electrical discharge machining process, part 2: surface integrity and roundness. J Manuf Sci Eng 124:708–714

25. Haddad MJ, Tehrani AF (2008) Material removal rate (MRR) study in the cylindrical wire electrical discharge turning (CWEDT) process. J Mater Process Technol 199(1–3):369–378. doi:10.1016/j.jmatprotec.2007.08.020
26. Haddad MJ, Alihoseini F, Hadi M, Hadad M, Tehrani AF, Mohammadi A (2010) An experimental investigation of cylindrical wire electrical discharge turning process. Int J Adv Manuf Technol 46(9–12):1119–1132. doi:10.1007/s00170-009-2171-z
27. Janardhan V, Samuel GL (2010) Pulse train data analysis to investigate the effect of machining parameters on the performance of wire electro discharge turning (WEDT) process. Int J Mach Tools Manuf 50(9):775–788. doi:10.1016/j.ijmachtools.2010.05.008
28. Lhiaubet C, Meyer RM (1981) Method of indirect determination of the anodic and cathodic voltage drops in short high-current electric discharges in dielectric liquid. J Appl Phys 52(6):3929–3934. doi:10.1063/1.329197
29. Wong YS, Rahman M, Lim HS, Han H, Ravi N (2003) Investigation of micro-EDM material removal characteristics using single RC-pulse discharges. J Mater Process Technol 140(1–3):303–307. doi:10.1016/S0924-0136(03)00771-4
30. Rajurkar KP, Pandit SM (1986) Formation and ejection of EDM debris. J Manuf Sci Eng 108(1):22–26. doi:10.1115/1.3187036
31. McGeough JA (1988) Advanced methods of machining. Chapman & Hall, London
32. Jilani ST, Pandey PC (1982) Analysis and modelling of EDM parameters. Precis Eng 4(4):215–221. doi:10.1016/0141-6359(82)90011-3
33. Yadav V, Jain VK, Dixit PM (2002) Thermal stresses due to electrical discharge machining. Int J Mach Tools Manuf 42(8):877–888. doi:10.1016/S0890-6955(02)00029-9
34. Shankar P, Jain VK, Sundarajan T (1997) Analysis of spark profiles during EDM process. Mach Sci Tech 1(2):195–217. doi:10.1080/10940349708945647
35. Kojima A, Natsu W, Kunieda M (2008) Spectroscopic measurement of arc plasma diameter in EDM. CIRP Ann: Manuf Technol 57(1):203–207. doi:10.1016/j.cirp.2008.03.097
36. Patel MR, Barrufet MA, Eubank PT, DiBitonto DD (1989) Theoretical models of the electrical discharge machining process. II. The anode erosion model. J Appl Phys 66(9):4104–4111. doi:10.1063/1.343995
37. Salonitis K, Stournaras A, Stavroupoulos P, Chryssolouris G (2009) Thermal modeling of the material removal rate and surface roughness for die-sinking EDM. Int J Adv Manuf Technol 40(3–4):316–323. doi:10.1007/s00170-007-1327-y
38. Kunieda M, Lauwers B, Rajurkar KP, Schumacher BM (2005) Advancing EDM through fundamental insight into the process. CIPR Ann 54(2):64–87. doi:10.1016/S0007-8506(07)60020-1
39. Hinduja S, Kunieda M (2013) Modelling of ECM and EDM processes. CIRP Ann: Manuf Technol 62(2):775–797. doi:10.1016/j.cirp.2013.05.011
40. Marafona J, Chousal JAG (2006) A finite element model of EDM based on the joule effect. Int J Mach Tools Manuf 46:595–602. doi:10.1016/j.ijmachtools.2005.07.017
41. ANSYS manuals version 12.0, ANSYS ™ Inc., USA
42. Tao J, Ni J, Shih AJ (2012) Modeling of the anode crater formation in electrical discharge machining. J Manuf Sci Eng 134:1–11. doi:10.1115/1.4005303
43. Alvarez JLG, Greene JE, Turkovich BFV (1973) Study of the electro-erosion phenomenon of Fe and Zn. J Manuf Sci Eng 95(4):965–971. doi:10.1115/1.3438276
44. Williams RE, Rajurkar KP (1991) Study of wire electrical discharge machined surface characteristics. J Mater Process Technol 28(1–2):127–138. doi:10.1016/0924-0136(91)90212-W
45. Huang CA, Hsu FY, Yao SJ (2004) Microstructure analysis of the martensitic stainless steel surface fine-cut by the wire electrode discharge machining (WEDM). Mater Sci Eng A 371(1–2):119–126. doi:10.1016/j.msea.2003.10.277
46. Li L, Guo YB, Wei XT, Li W (2013) Surface integrity characteristics in wire-EDM of Inconel 718 at different discharge energy. Procedia CIRP 6:220–225. doi:10.1016/j.procir.2013.03.046
47. Kuriakose S, Shunmugam MS (2004) Characteristics of wire-electro discharge machined Ti6Al4V surface. Mater Lett 58(17–18):2231–2237. doi:10.1016/j.matlet.2004.01.037